forests

MDPI

Article

A Technology of Forest Fire Smoke Detection Using Dual-Polarization Weather Radar

Mengfei Jiang [1], Miao Bai [1], Zhonghua He [2,*], Gaofeng Fan [2], Minghao Tang [3] and Zhuoran Liang [1]

[1] Hangzhou Meteorological Bureau, Hangzhou 310051, China; jiangmurphy273@gmail.com (M.J.); baimiaohz@sina.com (M.B.); zhuoran.liang.sh@gmail.com (Z.L.)
[2] Zhejiang Climate Center, Hangzhou 310056, China; fangf@cma.gov.cn
[3] Zhejiang Academy of Emergency Management Science, Hangzhou 310007, China; tongcody@outlook.com
* Correspondence: hezh@cma.gov.cn

Abstract

Forest fire risk is rising with climate warming, highlighting the need for timely monitoring and early warning. Satellite-based monitoring, currently a primary tool in remote sensing for fire detection, suffers from spatiotemporal gaps due to limited resolution and cloud cover. This study developed a novel smoke detection technology using operational S-band dual-polarization weather radar. By analyzing six forest fire cases in Zhejiang Province, China (2023), we established a filtering method using dual-polarization parameters, with thresholds set to a differential reflectivity (Z_{DR}) $\geq$ 3 dB and a cross-correlation coefficient (ρ_{HV}) $\leq$ 0.7. This method effectively isolates fire-related echoes and, compared with geostationary satellites, enables more continuous monitoring; it also detects small and early-stage fires. Furthermore, radar-derived fire perimeters closely match satellite imagery, demonstrating its potential for real-time fire-spread tracking. The high spatiotemporal resolution and multi-parameter advantages of dual-polarization radar can complement satellite observations, offering vital support for early warning and real-time decision-making in fire management.

Keywords: forest fire smoke; weather radar; dual-polarization; differential reflectivity; early warning

check for updates

Academic Editor: Viacheslav I. Kharuk

Received: 5 August 2025
Revised: 4 September 2025
Accepted: 15 September 2025
Published: 16 September 2025

Citation: Jiang, M.; Bai, M.; He, Z.; Fan, G.; Tang, M.; Liang, Z. A Technology of Forest Fire Smoke Detection Using Dual-Polarization Weather Radar. *Forests* **2025**, *16*, 1471. https://doi.org/10.3390/f16091471

Copyright: © 2025 by the authors. Licensee MDPI, Basel, Switzerland. This article is an open access article distributed under the terms and conditions of the Creative Commons Attribution (CC BY) license (https://creativecommons.org/licenses/by/4.0/).

1. Introduction

The frequency and probability of forest fire occurrences have continued to increase with global warming [1]. The occurrence of extreme wildfire events worldwide has risen by nearly 2.2 times from 2003 to 2023 [2]. Studies have shown that during the period from 2001 to 2023, climate change has led to a substantial increase in fire emissions in temperate forests. In particular, one temperate fire ecoregion spanning the boreal forests of Eurasia and North America has experienced nearly a twofold increase in fire-related emissions, primarily driven by climate-induced droughts and changes in vegetation [3]. Under the continued climate change caused by the greenhouse effect, it is projected that by the end of the century (2070–2100), the potential risk of wildfires will increase significantly, requiring greater investment in disaster prevention and post-fire recovery efforts in the future [4].

Although forest fires cannot be completely prevented, early detection and precise geolocation can significantly minimize their devastation [5]. Remote sensing remains a critical tool for forest fires monitoring [6], with methods classified into terrestrial-, airborne-, and spaceborne-based systems [7]. Commonly used technologies include satellite remote

sensing, unmanned aerial vehicles (UAVs), manned aviation platforms, fixed ground-based camera systems, and terrestrial sensor networks [8]. Each of these techniques presents its own advantages and limitations in terms of spatial coverage, response speed, deployment cost, and data timeliness [9]. Among these, satellite remote sensing has become indispensable means of conventional detection [10], with systems like USA's Moderate Resolution Imaging Spectroradiometers (MODIS) onboard Terra and Aqua satellites [11,12], Japan's Himawari-8/9 [13] and China's FengYun series satellites [14]. The primary advantages of satellites for wildfire detection lie in their cost-effectiveness, large-scale coverage, and continuous observation capability [9,15]. However, there are still some shortcomings for the satellites in forest fire monitoring; these include (1) struggling with spatial resolution (hundreds of meters to kilometers) and temporal gaps (hours between revisits for LEO satellites); (2) being more susceptible to cloud interference and only able to infer fire and smoke changes indirectly through pixel observations [16].

Weather radars are extensively used worldwide to monitor precipitation and severe weather, supported by a large, globally distributed observational network [17]. Compared to satellite sensors, weather radars could provide continuous, real-time tracking with finer resolution. For example, Doppler weather radars typically achieve radial resolutions of 150–300 m, depending on the pulse width, with range gate spacing commonly set at 250–500 m [18]. As a supplement, weather radar has been shown to detect forest fires, such as Melnikov et al. (2008) who demonstrated the detection of a forest fire plume during a 2006 wildfire in Oklahoma and showed that the radar signatures of the fire plume were clearly distinguishable even through cloud cover [19]. However, as reviewed by McCarthy et al. (2019), Radar-based wildfire research has progressed unevenly, with more emphasis on plume studies than operational monitoring systems—despite its potential utility in fire detection [20]. For instance, Lang et al. (2014) utilized dual-polarization radar to investigate the vertical velocity and microphysical characteristics of pyro-convective plumes in Colorado wildfires [21]. Additionally, the diversity of radar instruments and scanning strategies adopted across studies [20], this may have further hindered the development of systematic operational approaches for wildfire monitoring.

In recent years, research on weather radar-based wildfire detection has gained increasing attention, with growing efforts devoted to advancing systematic application studies that could support the operational use of this technology in wildfire monitoring. For example, Lareau et al. (2022) [22] successfully tracked the boundaries of two large wildfires using reflectivity data—one of which had a confirmed core area of 80 square kilometers—demonstrating the potential of radar for large-scale wildfire monitoring. However, its applicability to fires of other scales has not yet been verified [22]. Shu et al. (2023) developed a wildfire detection algorithm based on reflectivity, which underwent application-level validation, but its discrimination capability still has considerable room for improvement [23]. The above studies were limited to the use of a single reflectivity parameter and did not utilize the unique advantages of dual-polarization variables, resulting in limited capture of wildfire multidimensional features. In terms of the use of dual-polarization variables, Zrnic et al. (2020) analyzed multiple wildfire events and identified preliminary characteristics of wildfire smoke in radar dual-polarization parameters, including differential reflectivity (Z_{DR}) and cross-correlation coefficient (ρ_{HV}), and differential propagation phase (Φ_{DP}), providing a foundation for multidimensional understanding of wildfire smoke signals [24]. Krishna et al. (2024) estimated plume injection heights based on Z_{DR} and ρ_{HV}, preliminarily demonstrating the application potential of dual-polarization parameters in wildfire monitoring [25]. As a result, the integration of multiple parameters, especially dual-polarization variables, could be critical for investigating more stable and effective detection of wildfire.

However, due to the limitations of forest fire detection based solely on radar reflectivity [22,23], and dual-polarization have not been utilized in operational fire smoke detection, as previous studies focused only on analyzing their characteristics [24]. It is still challenging to accurately distinguish wildfire signal from complex radar echoes for its small spatial scale [20]. To address these issues, this study innovatively introduced dual-polarization parameters into actual forest fire smoke detection. A filtering method was developed based on the distinctive signatures of fire smoke echoes in differential reflectivity (Z_{DR}) and cross-correlation coefficient (ρ_{HV}), and a Forest Fire Intensity Index (FEI) index was proposed to dynamically track fire intensity. Overall, this study demonstrates a feasible approach and framework for forest fire smoke detection and monitoring using weather radar.

2. Materials and Methods

2.1. Study Area and Data

Zhejiang Province is located on the southern wing of the Yangtze River Delta along China's southeastern coast. It has a subtropical monsoon climate and is one of the provinces with the highest forest coverage in China; forest fires are one of the primary natural disasters affecting forest management in this region [26]. Related studies have indicated that the risk of forest fires in Zhejiang is relatively severe, with fires occurring annually and resulting in considerable damage [27]. Due to the unique geographical location and climatic conditions, the region is characterized by abundant moisture and frequent cloud activity [28,29], posing certain challenges to traditional satellite remote sensing for fire monitoring. In contrast, Zhejiang has a well-established weather radar network with high coverage, capable of all-weather, multi-angle detection. When utilized for forest fire monitoring, it has the potential to complement satellite remote sensing and support early warning systems in forest fire monitoring. In addition, the high incidence of forest fires in the region, together with the presence of a comprehensive dual-polarization weather radar network, provides sufficient observational data and case samples to support the present study.

This study selected six forest fire events that occurred in Zhejiang Province in 2023 as experimental samples; the details of these cases are listed in Table 1, and their geographical distribution along with the weather radar stations is shown in Figure 1. Fire point data were obtained from NASA Worldview's global daily fire dataset (NASA, Washington, DC, USA; https://worldview.earthdata.nasa.gov/, accessed on 11 October 2024) and verified by the Zhejiang Provincial Emergency Management Department. Weather radar data were provided by the Zhejiang Meteorological Bureau. To compare the detection capabilities of radar and satellite for forest fires, fire monitoring products from the Himawari-8/9 satellites were used. Furthermore, Sentinel-2 satellite imagery was employed to validate the correspondence between radar-detected smoke echoes and the actual smoke plumes.

Table 1. Forest Fire Cases: Date, Location, and Distance to Weather Radar.

No.	Date	Location	Longitude (°E)	Latitude (°N)	Distance (km)
1	6 March 2023	Yuhuan, Taizhou	121.34	28.26	30
2	4 March 2023	Xianju, Taizhou	120.65	28.72	82
3	5 March 2023	Wuyi, Jinhua	119.78	28.74	54
4	6 March 2023	Wuyi, Jinhua	119.78	28.73	54
5	7 March 2023	Yongkang, Jinhua	120.00	28.95	39
6	8 January 2023	Pan'an, Jinhua	120.43	28.98	85

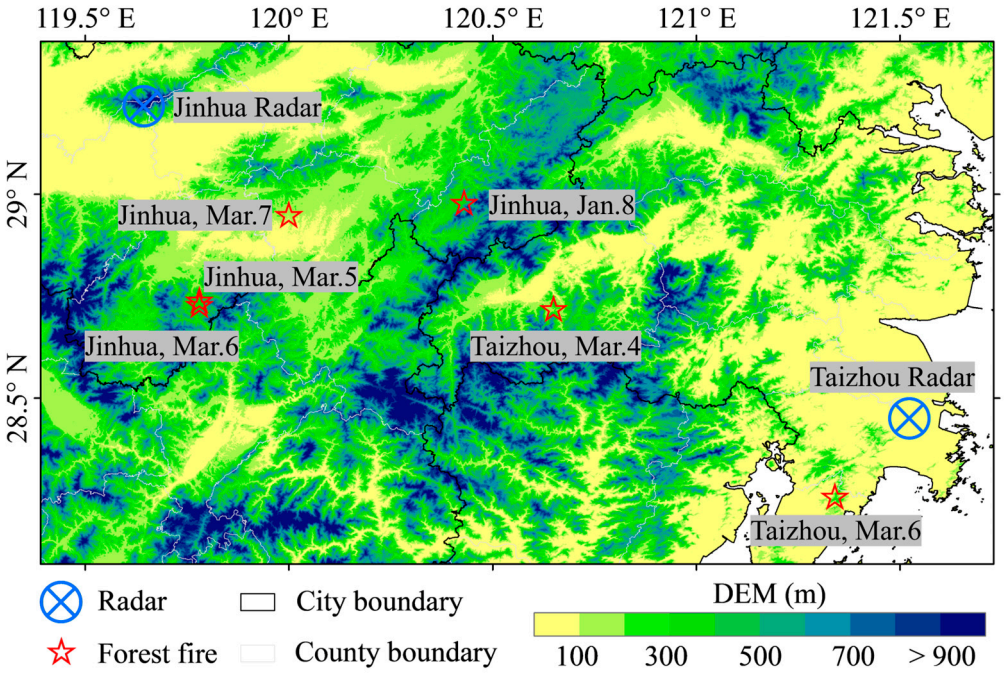

Figure 1. Location of Forest Fire Cases and Weather Radar Stations in the Study Area.

All times in this study are presented in Beijing Time (UTC+8) to align with the local time zone of the study area, thereby facilitating clearer and more intuitive interpretation of the timing of forest fire events.

2.1.1. Satellite Dataset

To assess detection performance, Himawari-8/9 satellite fire products were employed for comparison with radar-based continuous monitoring signals. These products are based on the Himawari Advanced Imager (AHI), which provides full-disk observations every 10 min, making them suitable for real-time fire analysis in East Asia. Fire detection mainly relies on brightness temperatures in the 3.9 μm and 10.8 μm bands to identify hotspots and distinguish them from the background. The derived Fire Radiative Power (FRP) reflects fire intensity. The spatial resolution is 2 km, corresponding to a pixel area of 4 km^2 [30].

Sentinel-2, launched by the European Space Agency (ESA), consists of two satellites—Sentinel-2A and Sentinel-2B. Since March 2017, the mission has achieved a global revisit cycle of five days. It provides multispectral imagery with a maximum spatial resolution of 10 m [31]. In this study, true-color composite images based on the blue, green, and red bands of Sentinel-2 data were used to observe forest fire sites and smoke conditions.

Himawari-8/9 satellite data can be obtained from the JAXA Himawari Monitor P-Tree System (Japan Aerospace Exploration Agency, Tokyo, Japan; https://www.eorc.jaxa.jp/ptree/, accessed on 27 May 2025), while Sentinel-2 satellite data are available via Google Earth Engine (Google LLC, Mountain View, CA, USA; https://earthengine.google.com/, accessed on 12 June 2025).

2.1.2. Dual-Polarization Weather Radar Data

This study employed S-band dual-polarization weather radar data from stations near the forest fire locations, provided by the Zhejiang Meteorological Bureau (Hangzhou, China). The data used were quality-controlled base data in standard single-site Doppler radar format, covering the full duration of each fire. All radars used were of the CINRAD/SAD type, primarily operating in the VCP21D precipitation scanning mode, which completes a volume scan of 9 elevation angles and 11 sweeps within 6 min. During strong

convective events, the VCP11D mode was adopted to improve vertical resolution. Products generated from the two volume coverage patterns are essentially equivalent [32], and the choice of scan mode does not affect forest fire echo detection.

Traditional single-polarization radars rely primarily on the reflectivity factor (Z) for forest fire detection [20]. However, the reflectivity of fire echoes often overlaps with that of precipitation echoes [33], requiring the use of indirect physical metrics such as the temporal variation in reflectivity or echo area, which limits both efficiency and reliability [23]. In contrast, dual-polarization parameters provide additional dimensions to directly characterize particle properties. These parameters help distinguish non-meteorological targets such as smoke and ash based on particle shape, size, and homogeneity [34]. Typical signatures include high Z_{DR}, low ρ_{HV}, and large Φ_{DP} [21,24,25]. Among them, low ρ_{HV} effectively separates fire echoes from precipitation echoes [33], relatively high Z_{DR} distinguishes them from most other non-meteorological echoes [34], and horizontal reflectivity (Z_H) can be combined to further suppress weak clutter [34–36]. Moreover, biological echoes, which may share certain features with fire echoes [24], are generally spatially discrete, less continuous [37], and typically confined below 200 m [38]. Therefore, dual-polarization radar has the potential to provide a more straightforward and efficient means of directly identifying forest fires.

2.2. Research Methods for Forest Fire Smoke Detection

Figure 2 presents the methodological flowchart for forest fire smoke detection based on dual-polarization weather radar. The main steps include (1) extraction of dual-polarization parameters and preliminary feature analysis to establish initial thresholds; (2) application of initial thresholds to perform dual-polarization filtering tests, followed by threshold optimization to develop the dual-polarization filtering method; and (3) extraction of forest fire echoes from radar data, and subsequent analysis and comparison of results using satellite data.

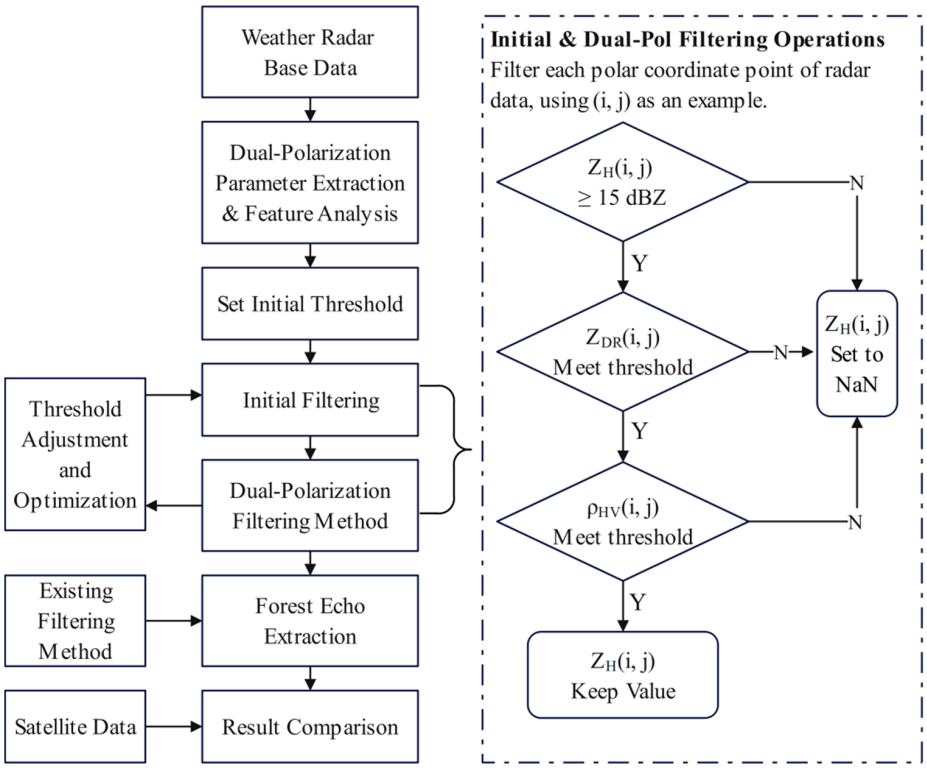

Figure 2. Flow-chart of research method.

2.2.1. Fire Echo Intensity Index

A Fire Echo Intensity Index (FEI) is proposed in this study to characterize the variation features of forest fire echoes as the fire evolves. This index is newly defined in this study, and its formulation is based on commonly used radar parameters. This index combines the number of coordinate points of radar forest fire echoes and the horizontal reflectivity (Z_H) intensity to quantify the spatial expansion and scattering characteristics of the fire. The formula for calculating FEI is as follows:

$$\text{FEI} = N \cdot 10^{\frac{\overline{Z_H}}{10}} \quad (1)$$

where N represents the number of coordinate points within the forest fire area that have Z_H values, i.e., the detected fire echo points. It reflects the spatial coverage of the fire and generally increases as the fire spreads. $\overline{Z_H}$ is the average Z_H (in dBZ) of all forest fire echo points. It characterizes the average intensity of the fire echoes and relates to combustion properties such as smoke concentration or flame intensity. $10^{\overline{Z_H}/10}$ where the average Z_H (in dBZ) is transformed into a linear reflectivity factor (with units of mm^6/m^3), which indicates the average scattering intensity at each coordinate point.

The physical significance of FEI lies in its integration of both the spatial extent and the echo intensity of forest fire returns, reflecting the total scattering effect of forest fire echoes. As the fire intensifies, increases in either N or $\overline{Z_H}$ will lead to a corresponding rise in the FEI.

2.2.2. Dual-Polarization Parameter Filtering Method

Firstly, Z_H, Z_{DR}, and ρ_{HV} were extracted from the radar base data to generate spatial distribution maps for analysis. By comparing fire-affected and non-fire regions, characteristic dual-polarization values were identified, allowing for the initial determination of Z_{DR} and ρ_{HV} thresholds.

Before dual-polarization parameter filtering is applied, an initial reflectivity factor threshold is set to suppress weak clutter echoes. As in this study, we focus on radar data from low elevation angles of 0.5° and 1.5°, since the top height of wildfire smoke plumes is mostly concentrated around 3 km [39]. At these low angles, radar data often contain echoes from ground objects, biological sources, or atmospheric turbulence, which interfere with fire echo detection. These non-meteorological echoes generally exhibit reflectivity values, rarely exceeding 20 dBZ, while forest fire plumes often have higher reflectivity values, which can reach up to 40 dBZ [34]. Supporting this distinction, the National Weather Service (2011) notes that radar reflectivities of 15 dBZ or higher generally indicate measurable precipitation, making 15 dBZ a practical reference threshold for distinguishing non-meteorological echoes [35]. Accordingly, the initial reflectivity factor threshold is set to 15 dBZ.

Following the initial clutter removal, the dual-polarization parameter filtering was applied. The key to dual-polarization parameter filtering lies in the appropriate selection of thresholds. Previous studies have shown that although different types of echoes tend to cluster within specific ranges of dual-polarization parameters (e.g., Z_{DR} and ρ_{HV}), their observations may still be scattered across the full range [33]. Forest fire echoes exhibit similar behavior, but their concentration ranges are distinct from those of other types of clutter [24]. Based on this, we first analyzed the distributions of Z_{DR} and ρ_{HV} under fire conditions to propose an initial threshold range. This range was then progressively refined by systematically comparing the filtering outcomes under different thresholds. Through this process, a final discriminant threshold was determined that allows forest fire echoes to be clearly distinguished in the reflectivity field. The resulting filtering strategy prioritizes

the accurate identification and localization of forest fire echoes, while also striving to preserve their intensity and spatial extent. This approach comes at the cost of reduced recall, but effectively enhances clutter suppression. When higher detail is required (e.g., for fire boundary delineation), complete fire echo segments can be retrieved using the spatial extent.

At the operational level, this filtering method is implemented by applying all thresholds to each polar coordinate sampling point in the radar data. Points that satisfy all thresholds are retained to isolate forest fire echoes from background noise.

3. Forest Fire Monitoring Using Dual-Polarization Radar: A Case Study

On 6 March 2023, a forest fire broke out in Taizhou, Zhejiang Province, triggered by illegal burning of weeds by local villagers. Based on meteorological observations, at the time of the incident, there was no precipitation, and the preceding period had experienced low rainfall, and the on-site wind speed was 4–5 on the Beaufort scale. Combined with strong winds, the fire spread rapidly, affecting a large area and threatening several nearby villages. The fire site was approximately 30 km from the Taizhou weather radar station. According to the radar beam height formula [18], the radar beam heights at 0.5° and 1.5° elevation angles are approximately 0.3 km and 0.8 km, respectively—both within the typical height of wildfire smoke plumes [39].

Crucially, this event generated an exceptionally large and persistent smoke plume due to its extensive coverage, providing an ideal dataset to investigate the radar characteristics of forest fire smoke. Furthermore, the wind-driven spread of the fire also provided valuable data for studying dynamic fire evolution using radar. Additionally, the Sentinel-2 satellite successfully captured imagery of the smoke during the fire, providing an independent data source for comparison that can be used to validate findings related to fire location and smoke extent. Based on these unique observational advantages, this fire event was selected as a representative case for analysis in this study.

3.1. Polarimetric Feature Extraction and Forest Fire Echo Filtering

Figure 3 illustrated the distributions of multiple radar parameters at 0.5° and 1.5° elevation angles during the forest fire event of Taizhou on 6 March 2023, at 14:40 (UTC+8), a period marked by intense smoke plume activity. In the initial base reflectivity images (Figure 3a,d), the forest fire echoes are intermixed with substantial clutter, especially at the 0.5° elevation angle where clutter interference is more severe. Although the reflectivity values of the fire echoes are slightly higher than the surrounding clutter, their spatial scale is relatively small, making them difficult to distinguish from clutter.

In contrast, the Z_{DR} (Figure 3b,e) and ρ_{HV} (Figure 3c,f) distributions reveal certain distinct features in fire-affected areas. However, due to the large variability and uneven distribution of values within the region, these characteristic values are relatively ambiguous and it is difficult to directly determine specific threshold ranges. Specifically, the ρ_{HV} is concentrated below 0.75 in most forest fire areas, while the Z_{DR} exhibits relatively high values, exceeding 2.5 dB. Since no single parameter can completely distinguish forest fire echoes from other non-target echoes, a multi-parameter approach with combined thresholds is adopted.

Figure 4 presents boxplots of the two polarimetric parameters within the fire-affected region. The results indicate a typical pattern of high Z_{DR} and low ρ_{HV}, with median values of 2.25 dB and 0.635, respectively. Based on this characteristic range, different thresholds were applied to examine the influence of threshold selection on the filtering results.

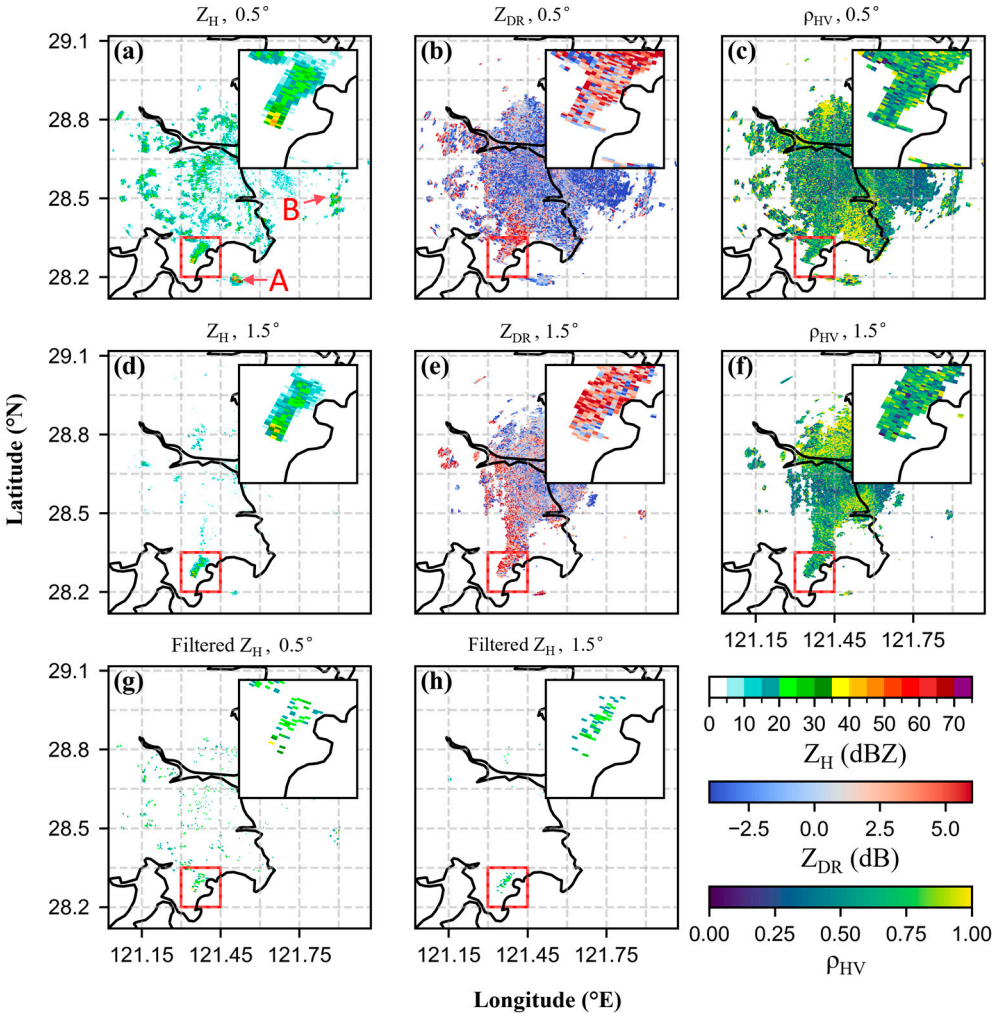

Figure 3. Dual-polarization radar parameters and filtered fire echoes at 0.5° and 1.5° elevation angles during the Taizhou forest fire. (**a**–**c**) Z_H, Z_{DR} and ρ_{HV} at 0.5° elevation; (**d**–**f**) Z_H, Z_{DR} and ρ_{HV} at 1.5° elevation; (**g**,**h**) Filtered Z_H at 0.5° and 1.5° elevation angles.

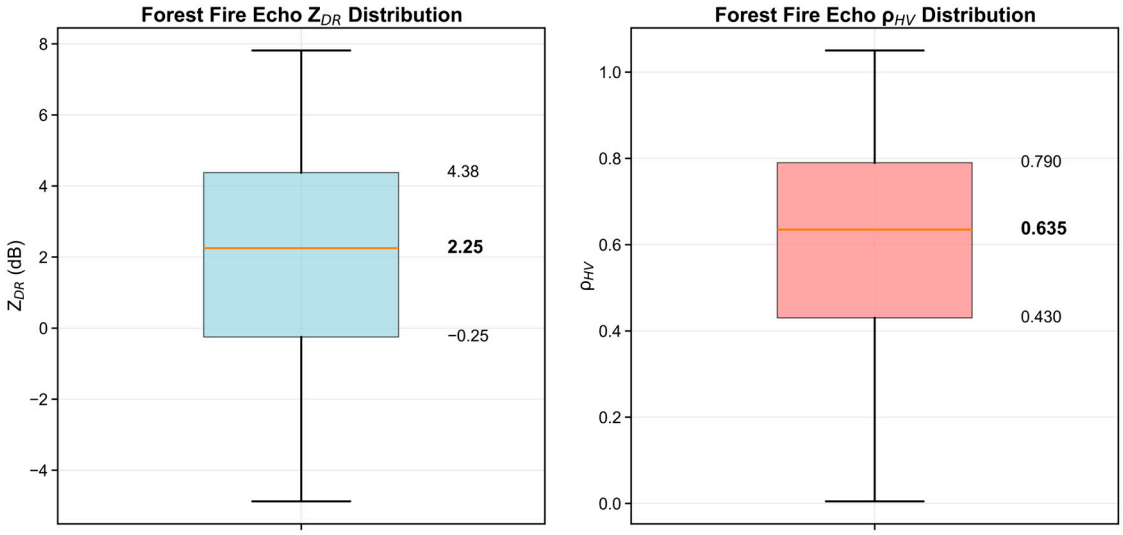

Figure 4. Box plots showing the distribution of Z_{DR} and ρ_{HV} values associated with forest fire events.

A heatmap of non-forest-fire echo removal rate versus forest fire echo retention rate was generated (Figure 5). The proportions are averaged results based on the filtering

outcomes of all radar data during the fire period. Results indicate that raising the Z_{DR} threshold or lowering the ρ_{HV} threshold increases clutter suppression but at the cost of removing true fire echoes. Excessive filtering risks weakening or eliminating key signal features, while insufficient filtering leaves clutter that masks fire signatures. Since the filtering ratio alone could not fully capture these trade-offs, the evaluation also relied on qualitative assessment of the filtered outcomes across different stages and threshold settings. These tests showed that thresholds around $Z_{DR} \geq 3$ dB and $\rho_{HV} \leq 0.7$ strike a relative balance, effectively suppressing clutter while keeping forest fire echoes clearly identifiable and preserving their intensity and spatial distribution compared with the original observations. Accordingly, the final thresholds were set to $Z_{DR} \geq 3$ dB and $\rho_{HV} \leq 0.7$, and the filtered results are shown in Figure 3g,h.

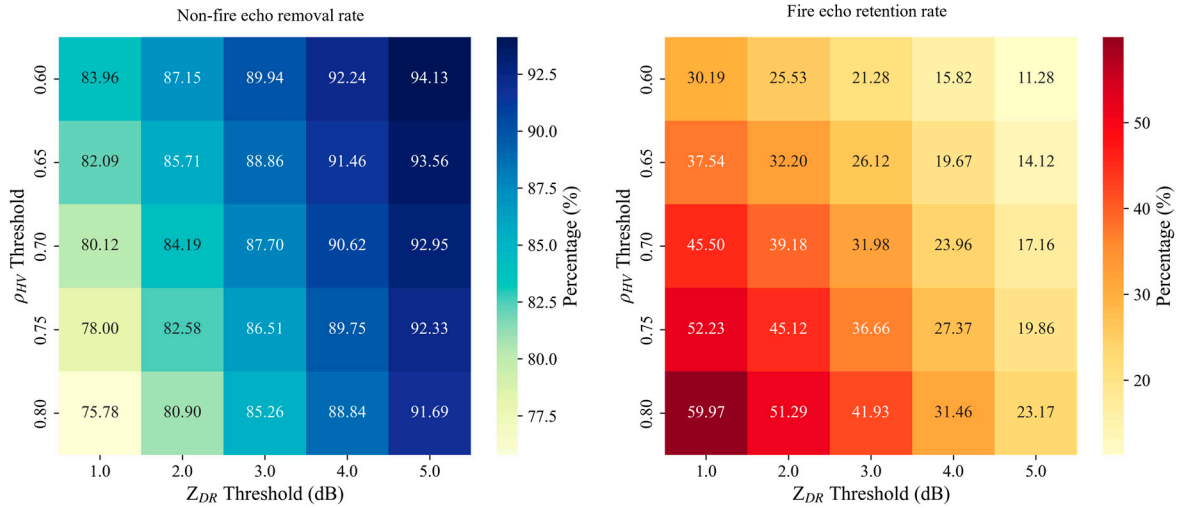

Figure 5. Heatmap of non-fire echo removal rate versus forest fire echo retention rate under varying Z_{DR} and ρ_{HV} thresholds.

Figure 3g and 3h, respectively, show the forest fire echo filtering results at the two elevation angles under the specified threshold conditions. It can be seen that the filtering effect at the 1.5° elevation angle is significant, with non-forest-fire echoes largely removed, and the retained forest fire echo regions concentrated and well-defined, facilitating easy identification. Meanwhile some scattered clutter echoes still exist at the 0.5° elevation angle, but these echoes are small in scale and sparsely distributed, clearly distinguishable from the forest fire echoes, thus allowing for further identification. Overall, the filtering process effectively preserves both the intensity and spatial structure of the forest fire echoes.

Notably, the two clutter echo patches indicated by arrows A and B in Figure 3a exhibit reflectivity values and spatial sizes very similar to that of the forest fire echo, making it difficult to distinguish them based on reflectivity alone. However, after applying dual-polarization filtering, both clutter regions were effectively removed, as shown in Figure 3g, demonstrating that incorporating dual-polarization parameters provides multidimensional recognition of forest fire smoke characteristics, and a stronger capability for identifying forest fire echoes, thus confirming the added value of multi-parameter screening in enhancing fire echo discrimination.

For implementation, Z_H, Z_{DR}, and ρ_{HV} were extracted from the radar base data and integrated into a unified xarray dataset. The combined condition ($Z_H \geq 15$ dBZ, $Z_{DR} \geq 3$ dB, $\rho_{HV} \leq 0.7$) can be efficiently applied across all grid points. Field tests demonstrated that this method enables efficient filtering operations and shows strong potential to meet the demands of dynamic, continuous, and real-time monitoring, effectively supporting the real-time identification and analysis of forest fire echoes.

3.2. Dynamic Tracking of Forest Fire Echoes and Comparison with Satellite Observations

To investigate the evolution characteristics of weather radar echoes during the forest fire event, this study presents time-sequence echo maps at several key stages of the fire, as shown in Figure 6. Since dual-polarization filtering may result in partial signal loss, fire-related echo regions were first identified based on the filtered results to determine the fire's location and extent. Accordingly, the complete echoes were finally re-extracted from the radar base data to provide a more comprehensive depiction of the fire evolution.

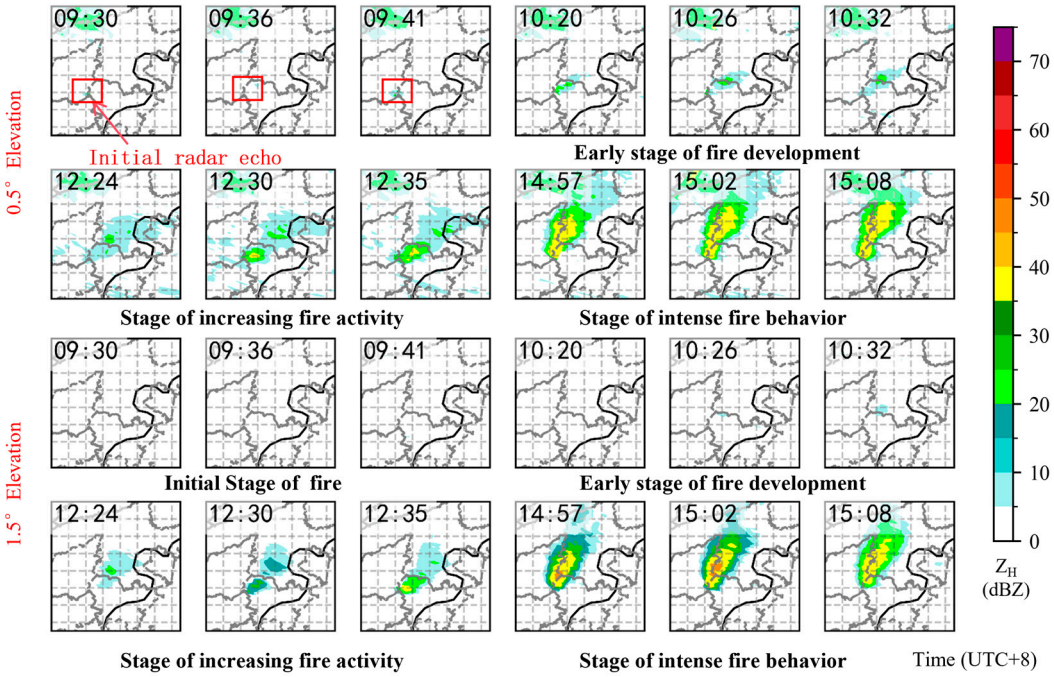

Figure 6. Time Series Chart of Radar Echoes for Forest Fire at Different Stages.

Weak echoes first appeared around 09:30 (UTC+8), gradually expanding from southwest to northeast. By 10:26, banded structures were observed at the 0.5° elevation angle. From 12:30 onward, echo intensity increased markedly, with values exceeding 35 dBZ at 0.5°, and stronger returns also emerging at 1.5°, centered near the original echo region. By approximately 15:00, the fire had intensified significantly, producing sustained, banded echoes with extensive high-reflectivity areas at both angles. Reflectivity at 1.5° exceeded 45 dBZ.

These observations indicate that forest fire echoes exhibit notable variations at different stages, with dynamic changes in spatial structure, boundary morphology, development direction, and intensity corresponding to the fire's progression.

Building on this, we compared radar data with Sentinel-2 satellite imagery captured during the fire (Figure 7) to assess the practical value of radar observational features for forest fire monitoring. The satellite imagery shows a banded southwest–northeast distribution of fire smoke, with spatial patterns broadly consistent with radar echoes at corresponding times (Figure 6).

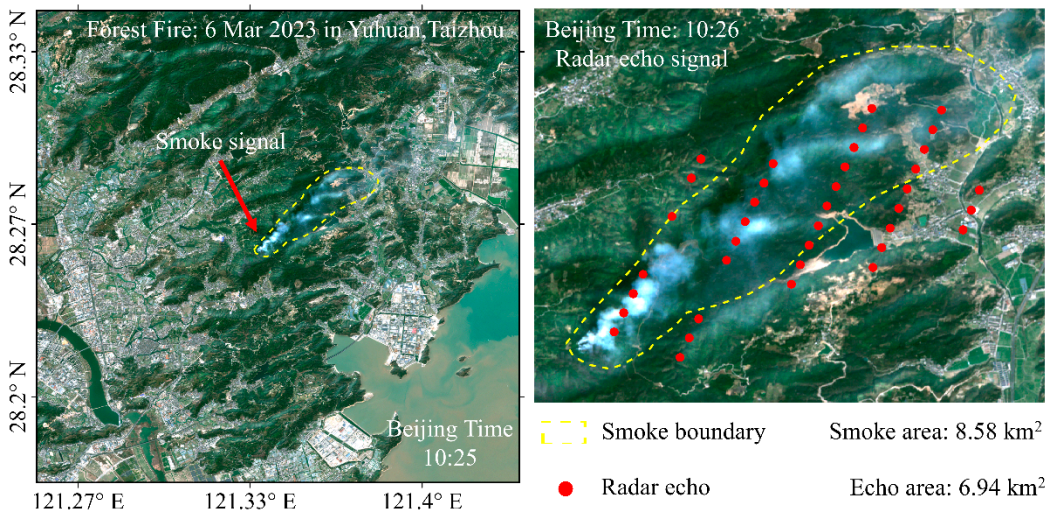

Figure 7. Characteristics of Forest Fire Smoke detected by Sentinel-2 Satellite and corresponding Radar Echo Signal.

Further comparison between radar echoes and satellite imagery shows that both can effectively reveal several key fire features, which are of significant value for dynamic fire monitoring and early warning. These are mainly reflected in the following four aspects:

1. Directional feature: Both radar reflectivity maps and satellite images show that the forest fire smoke and echoes are distributed in a banded pattern extending from southwest to northeast, indicating a clear direction of fire spread. Weather radar's continuous observation capability enables real-time tracking of fire spread paths, supporting rapid prediction of fire propagation trends.
2. Intensity feature: The satellite imagery indicate that the area near the smoke origin has the highest concentration, corresponding well with the actual fire location (121.34° E, 28.26° N). At the corresponding time, the strongest radar echo appears at the southwest end, with a maximum value at (121.341° E, 28.269° N), which is highly consistent with the actual fire point. This consistency demonstrates the radar's ability to accurately identify high-intensity fire regions, providing a basis for fire source localization and fire intensity assessment.
3. Diffusion feature: Satellite imagery shows the smoke spreading along the propagation direction and expanding sideways, a pattern also observed in radar echo maps. Radar's high-frequency detection can capture this diffusion in real time, aiding in understanding fire spread dynamics.
4. Boundary feature and quantitative estimation capability: Satellite imagery, with boundary extracted via ArcGIS (yellow dashed line, Figure 7), estimate smoke coverage at 8.58 km^2. Radar image echo points (red dots, Figure 7) align closely with this region. By summing radar resolution cell areas in polar coordinates, derived from radar data, the echo coverage is estimated at 6.94 km^2. The errors mainly stem from systematic errors of the satellite and radar systems, including satellite non-orthorectification errors [40] and radar effects such as Earth's curvature and atmospheric refraction [18]. Additional discrepancies arise from manual delineation of smoke boundaries in satellite imagery and from approximating radar echo areas using range-bin equivalence. The close agreement between these two estimates indicates that weather radar has the capability for quantitative delineation and estimation of fire smoke extent, demonstrating its potential for further outlining fire boundaries in fire monitoring.

In summary, the proposed dual-polarization filtering method enables continuous and dynamic extraction of forest fire-related echoes, clearly revealing their spatiotemporal evolution. Comparison with Sentinel-2 satellite imagery confirms the consistency between radar-derived features and actual fire conditions, highlighting the method's application potential in real-world fire monitoring. Leveraging the high spatiotemporal resolution of weather radar, this approach provides essential support for dynamic monitoring, quantitative analysis, and early warning of forest fires, demonstrating strong prospects for further application.

4. Forest Fire Monitoring Application

4.1. Application of Dual-Polarization Filtering in Multiple Forest Fires

To further validate the reliability of the threshold settings and the applicability of the dual-polarization parameter-based filtering method, this study selected five distinct forest fire cases to evaluate the radar echo filtering performance. Figure 8a–e illustrate the base reflectivity maps of each case, showing comparisons before and after the dual-polarization filtering process. The results demonstrate that the proposed method effectively removes non-forest-fire echoes, significantly improving the clarity of forest fire echoes and enabling rapid and accurate identification of fire-affected areas.

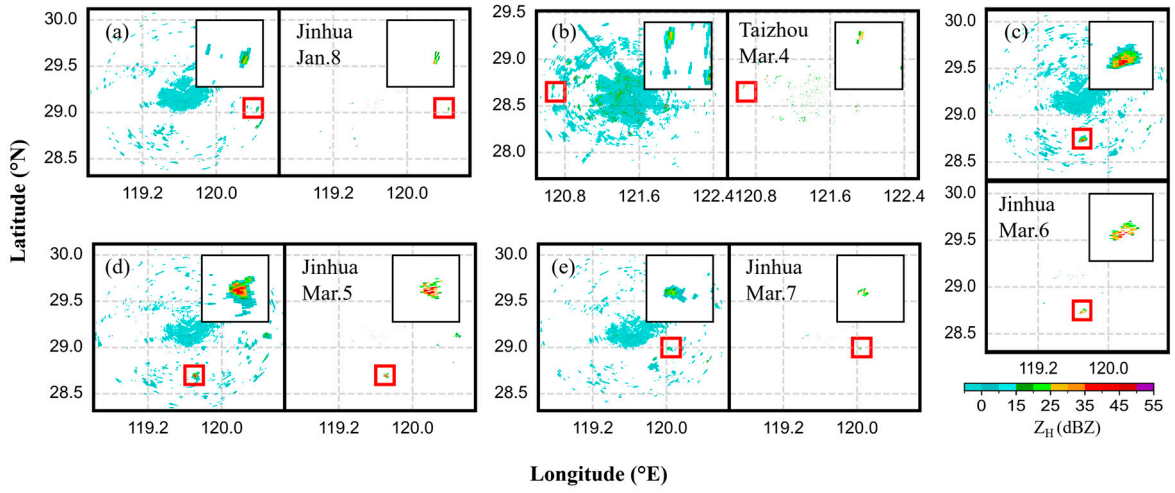

Figure 8. Radar Echoes Before and After Filtering in Multiple Forest Fires. (**a**) Jinhua, 8 January; (**b**) Taizhou, 4 March; (**c**) Jinhua, 5 March; (**d**) Jinhua, 6 March; (**e**) Jinhua, 7 March.

Notably, in the cases of Jinhua on 8 January, Taizhou on 4 March, and Jinhua on 7 March 2023, where the fire echoes were relatively small in spatial extent, the filtered reflectivity maps still clearly showed distinct forest fire smoke echo signals (see Figure 8a,b,e). These findings demonstrate that the dual-polarization filtering approach not only enables effective extraction of forest fire echoes but also shows the capability to identify smaller-scale fire events.

4.2. Comparative Analysis of Radar and Satellite Signals for Forest Fire Monitoring

Table 2 compares the initial detection times of forest fires across multiple cases, with radar detections based on the dual-polarization filtering method and satellite detections. Except for the fire in Xianju, Taizhou on 4 March 2023—where the radar detected the fire 7 min later than the satellite—all other cases show that radar identified fire-related signals earlier than the satellite. Notably, during the fire in Yuhuan, Taizhou on 6 March 2023, radar began detecting wildfire echoes as early as 09:30, while the satellite's first detection occurred at 15:02, resulting in a lead time of over five hours, though such a large lead in

a single case may involve some degree of randomness. Considering that Himawari-8/9 typically experiences a data latency of 15–20 min [41], while radar observations are almost real-time, these experimental results showed that radar detects forest fire onset earlier than satellite data.

Table 2. Comparative Analysis of Initial Detection Times Between Radar and Satellite in Multiple Forest Fire Cases.

No.	Date	Location	Radar	Satellite	Time Difference
1	6 March 2023	Yuhuan, Taizhou	9:30	15:02	>5 h
2	4 March 2023	Xianju, Taizhou	14:30	14:23	−7 min (Close)
3	5 March 2023	Wuyi, Jinhua	12:24	13:04	40 min
4	6 March 2023	Wuyi, Jinhua	12:50	13:04	14 min
5	7 March 2023	Yongkang, Jinhua	15:16	17:11	115 min
6	8 January 2023	Pan'an, Jinhua	14:18	14:45	27 min

To further compare the temporal evolution and dynamic performance of radar and satellite signals during forest fires, this study introduces the Fire Echo Intensity Index (FEI), defined in Section 2.2.1. FEI quantifies fire intensity variations from both spatial extent and echo strength perspectives, providing a robust tool for the quantitative analysis of radar echoes. Due to the large range of FEI values, logarithmic transformation was applied to compress the range while preserving its variation characteristics. This facilitates visualization alongside satellite observations.

It is important to note that the radar echoes used in FEI computation are not raw reflectivity data, but rather forest fire characteristic signals extracted using the dual-polarization filtering method developed in this study. Therefore, FEI represents the spatial and temporal intensity of forest fire-related features, effectively excluding non-meteorological clutter and background noise.

Figure 9 illustrates the temporal variation in radar signals logFEI and satellite Fire Radiative Power (FRP) for six forest fire cases. Different symbols denote valid radar or satellite detections at each time point, with lines connecting consecutive points to show continuous monitoring.

Overall, radar signals demonstrate strong continuity and stability, typically rising sharply at fire onset, maintaining high levels throughout, and gradually weakening or becoming sporadic near the end, highlighting radar's robust dynamic monitoring capability. In contrast, satellite observations are often intermittent or missing during fire events, limiting continuous fire tracking.

Additionally, satellite signals typically appear following a notable rise in radar signals, reflecting radar's higher sensitivity to early-stage fires.

Notably, radar and satellite observations display similar temporal trends, albeit with pronounced short-term fluctuations in both. This consistency is particularly evident during the periods marked by the red dashed boxes in Figure 9a,b. This alignment is further corroborated by linear correlation analysis (Figure 10), where radar data are aligned to satellite timestamps by averaging radar values within 5 min before and after each satellite observation (a 10 min window): the aligned signals (Figure 10a,c) exhibit moderate correlation, whereas after applying a 5-point smoothing, the radar and satellite intensity variations reveal a strong linear relationship, with R values reaching 0.92 for one case and 0.83 for the other. These results confirm that the FEI effectively reflects fire intensity evolution and serves as a reliable metric for radar-based fire monitoring.

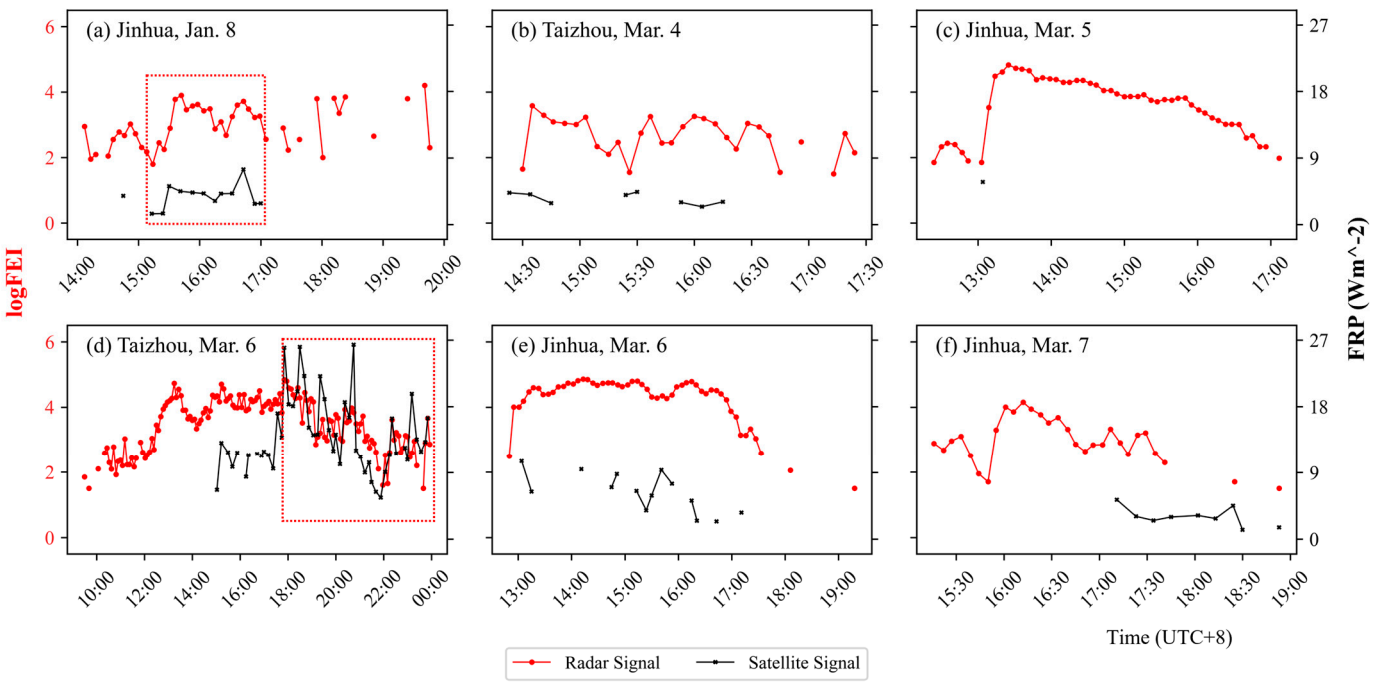

Figure 9. Temporal evolution of radar and satellite signals in multiple forest fire cases. (**a**) Jinhua, 8 January; (**b**) Taizhou, 4 March; (**c**) Jinhua, 5 March; (**d**) Taizhou, 6 March; (**e**) Jinhua, 6 March; (**f**) Jinhua, 7 March.

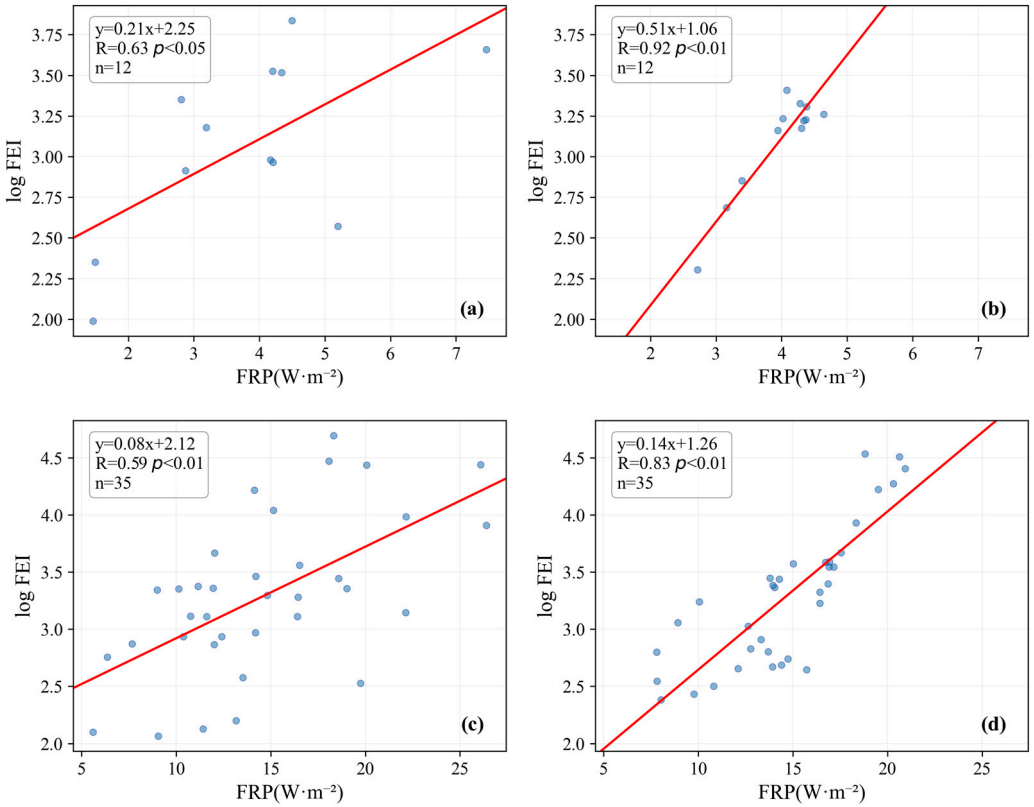

Figure 10. The linear correlation analysis of logFEI and FRP: (**a**,**b**) before and after 5-point smoothing, Jinhua, 8 January; (**c**,**d**) before and after 5-point smoothing, Taizhou, 6 March.

Therefore, the Fire Echo Intensity Index (FEI), derived from radar echoes extracted via the dual-polarization filtering method, can effectively capture the dynamic evolution of forest fire intensity. Furthermore, compared to satellite observations, radar signals offer

superior temporal continuity and stability throughout the fire life cycle, enabling more consistent and reliable monitoring of fire progression. These advantages highlight the potential of weather radar, combined with the proposed dual-polarization filtering approach, as a powerful tool for continuous, real-time forest fire detection and intensity assessment.

5. Discussion

5.1. Physical Origins of Radar Signals and Differences from Satellite Observation Mechanisms

Previous studies have shown that wildfire smoke plumes contain a large number of non-spherical suspended particles, which exhibit detectable polarimetric characteristics. Their asymmetric structures and diverse morphologies result in significantly positive Z_{DR} and relatively low ρ_{HV} signatures [42,43]. These particles can be transported over long distances within the fire plume and tend to maintain their polarimetric signatures under aerodynamic forces [44], making them identifiable in dual-polarization radar observations [24].

In this study, by applying threshold filtering based on dual-polarization parameters, forest fire-related radar echoes were successfully extracted. The temporal evolution of the Fire Echo Intensity (FEI) index—marked by a rapid rise during the early plume ascent (due to a sharp increase in particle concentration) and a gradual decline in the later stage (as buoyancy weakens and particles settle)—reflects the dynamic manifestation of these physical characteristics. This indicates that the radar signals primarily originate from smoke and ash particles of forest fires.

Compared with satellite-based systems that rely on thermal infrared emissions from surface hotspots, active fires must reach a minimum fire radiative power (FRP) threshold, below which they are undetectable [16]. Radar detects the physical scattering responses of suspended particulates, including particles from early-stage smoke and ash, thereby offering enhanced capability for detecting weak or early-stage fires [22]. This advantage is particularly pronounced under cloud-covered conditions, where radar demonstrates better penetration performance [19]. The combined use of dual-polarization parameters and the FEI index provides a robust physical basis for continuous, life-cycle monitoring of forest fires.

5.2. Limitations of the Dual-Polarization Filtering Method

In this study, several important limitations should be noted:

1. Ground clutter cannot be fully eliminated at the 0.5° elevation angle, which constitutes a key limitation of this study. Although the dual-polarization filtering method performed well overall across the six cases, some residual clutter remained due to the overlap between the polarimetric signatures of clutter and fire-related echoes—for example, ground clutter typically exhibits Z_{DR} values distributed across its full range [45]. Under conditions of ambiguous boundaries or overlapping signals, fixed-threshold methods may struggle to fully distinguish fire echoes from non-meteorological noise. To balance the completeness of fire signals and filtering accuracy, the current strategy adopts conservative parameter settings, allowing limited residual clutter. This issue was particularly evident in the two Taizhou cases (Figures 3g and 8b), both of which were observed by the same radar station. By overlaying high-resolution ASTER GDEM V3 elevation data (30 m spatial resolution), we found that approximately 41.6% of the residual clutter pixels in the 6 March case corresponded to terrain elevations above the radar beam height. Combined with the substantial reduction in clutter at the 1.5° elevation angle, this supports the inference that the clutter is primarily caused by terrain blockage.

2. Limitations of Threshold Selection: although the selection of dual-polarization parameter thresholds is based on experimental analysis, it still relies on empirical judgment and manual trade-offs, which limits its general applicability. While the threshold combination has been validated in additional wildfire cases, the number of validation samples remains limited and the study area is relatively concentrated; therefore, its applicability under different geographical settings, terrain conditions, and fire types requires further verification.
3. Limitations in FEI Validation: although the proposed Fire Echo Intensity (FEI) index effectively captures the long-term evolution of fire intensity and exhibits high consistency with satellite observations, it lacks direct validation using high spatiotemporal resolution ground-based measurements. In particular, its capability to characterize short-term fluctuations in fire intensity has not yet been fully assessed.

5.3. Future Work and Outlook

(1) Addressing current limitations:

This study demonstrates the feasibility of using dual-polarization radar for forest fire monitoring; however, several limitations remain. Future research may incorporate additional polarimetric variables beyond Z_H, Z_{DR} and ρ_{HV} to better characterize the multi-dimensional signatures of wildfire plumes, such as differential propagation phase (Φ_{DP}), radial velocity (V_r) and spectrum width (σ_v), all of which have been shown to exhibit characteristic signatures in wildfire echoes [24]. Furthermore, instead of using empirically fixed thresholds, machine-learning or deep-learning approaches could be developed to automatically determine optimal classification thresholds under varying environmental conditions. The proposed Fire Echo Index (FEI) may also be refined by integrating higher-resolution ground-based wildfire observations (e.g., in situ sensors or UAV data) to enhance its capability in representing fire-intensity dynamics.

(2) Expanding potential applications:

The findings of this study reveal that weather radar can not only detect forest fire plumes but also locate fire sources and estimate plume areas. Future work could leverage this capability by coupling radar-derived plume extent with meteorological data to simulate smoke dispersion and infer the spatial extent of active fire zones. Such integration would provide a more comprehensive assessment of wildfire evolution and valuable information for emergency response and fire management.

6. Conclusions

This study proposes a dual-polarization radar filtering method based on differential reflectivity (Z_{DR}) and correlation coefficient (ρ_{HV}) for effective extraction of forest fire smoke echoes. Application to six forest fire cases demonstrates the method's good adaptability and identification performance, enabling stable and continuous monitoring of fire evolution, particularly during early fire stages. Additionally, the extracted radar signatures show potential for fire localization and fire spread trend analysis.

These findings highlight the potential of dual-polarization radar for continuous monitoring of forest fires, demonstrating a novel application of weather radar in forest fire detection, while several limitations remain to be addressed in future research.

Author Contributions: Conceptualization, M.J. and Z.H.; methodology, M.J. and M.B.; software, M.J.; validation, M.J., M.T. and Z.H.; formal analysis, M.J.; investigation, M.B.; resources, M.T.; data curation, M.J. and M.B.; writing—original draft preparation, M.J.; writing—review and editing, Z.H. and Z.L.; visualization, M.J. and Z.H.; supervision, Z.L. and G.F.; project administration, G.F.; funding acquisition, G.F. All authors have read and agreed to the published version of the manuscript.

Funding: This research was funded by the following grants: "Pioneer" and "Leading Goose" R&D Program of Zhejiang (Grant No. 2023C03190); Zhejiang Emergency Management Research and Development Project (Grant No. 2024YJ015); Science and Technology of Zhejiang Meteorological Bureau (Grant No. 2023ZD08 and 2023QN17).

Data Availability Statement: The original contributions presented in this study are included in the article. Further inquiries can be directed to the corresponding authors.

Conflicts of Interest: The authors declare no conflicts of interest.

Abbreviations

The following abbreviations are used in this manuscript:

Z_H	Horizontal Reflectivity Factor
Z_{DR}	Differential Reflectivity
ρ_{HV}	Correlation Coefficient
FEI	Fire Echo Intensity Index
FRP	Fire Radiative Power

References

1. Ellis, T.M.; Bowman, D.M.J.S.; Jain, P.; Flannigan, M.D.; Williamson, G.J. Global Increase in Wildfire Risk Due to Climate-Driven Declines in Fuel Moisture. *Glob. Change Biol.* **2022**, *28*, 1544–1559. [CrossRef]
2. Cunningham, C.X.; Williamson, G.J.; Bowman, D.M.J.S. Increasing Frequency and Intensity of the Most Extreme Wildfires on Earth. *Nat. Ecol. Evol.* **2024**, *8*, 1420–1425. [CrossRef]
3. Jones, M.W.; Veraverbeke, S.; Andela, N.; Doerr, S.H.; Kolden, C.; Mataveli, G.; Pettinari, M.L.; Le Quéré, C.; Rosan, T.M.; van der Werf, G.R.; et al. Global Rise in Forest Fire Emissions Linked to Climate Change in the Extratropics. *Science* **2024**, *386*, eadl5889. [CrossRef] [PubMed]
4. Liu, Y.; Stanturf, J.; Goodrick, S. Trends in Global Wildfire Potential in a Changing Climate. *For. Ecol. Manag.* **2010**, *259*, 685–697. [CrossRef]
5. Payra, S.; Sharma, A.; Verma, S. Application of Remote Sensing to Study Forest Fires. In *Atmospheric Remote Sensing*; Elsevier: Amsterdam, The Netherlands, 2023; pp. 239–260.
6. Mohapatra, A.; Trinh, T. Early Wildfire Detection Technologies in Practice—A Review. *Sustainability* **2022**, *14*, 12270. [CrossRef]
7. Barmpoutis, P.; Papaioannou, P.; Dimitropoulos, K.; Grammalidis, N. A Review on Early Forest Fire Detection Systems Using Optical Remote Sensing. *Sensors* **2020**, *20*, 6442. [CrossRef]
8. Szpakowski, D.M.; Jensen, J.L.R. A Review of the Applications of Remote Sensing in Fire Ecology. *Remote Sens.* **2019**, *11*, 2638. [CrossRef]
9. Honary, R.; Shelton, J.; Kavehpour, P. A Review of Technologies for the Early Detection of Wildfires. *ASME Open J. Eng.* **2025**, *4*, 040803. [CrossRef]
10. Allison, R.S.; Johnston, J.M.; Craig, G.; Jennings, S. Airborne Optical and Thermal Remote Sensing for Wildfire Detection and Monitoring. *Sensors* **2016**, *16*, 1310. [CrossRef]
11. Giglio, L.; Schroeder, W.; Justice, C.O. The Collection 6 MODIS Active Fire Detection Algorithm and Fire Products. *Remote Sens. Environ.* **2016**, *178*, 31–41. [CrossRef]
12. Giglio, L.; Boschetti, L.; Roy, D.P.; Humber, M.L.; Justice, C.O. The Collection 6 MODIS Burned Area Mapping Algorithm and Product. *Remote Sens. Environ.* **2018**, *217*, 72–85. [CrossRef]
13. Zhang, L.; Zhang, Q.; Yang, Q.; Yue, L.; He, J.; Jin, X.; Yuan, Q. Near-Real-Time Wildfire Detection Approach with Himawari-8/9 Geostationary Satellite Data Integrating Multi-Scale Spatial–Temporal Feature. *Int. J. Appl. Earth Obs. Geoinf.* **2025**, *137*, 104416. [CrossRef]
14. Yang, J.; Zhang, Z.; Wei, C.; Lu, F.; Guo, Q. Introducing the New Generation of Chinese Geostationary Weather Satellites, Fengyun-4. *Bull. Am. Meteorol. Soc.* **2017**, *98*, 1637–1658. Available online: https://journals.ametsoc.org/view/journals/bams/98/8/bams-d-16-0065.1.xml (accessed on 21 July 2025). [CrossRef]
15. Tian, X.-R.; McRae, D.J.; Li, S.-F.; Wang, M.-Y.; Li, H. Satellite Remote-Sensing Technologies Used in Forest Fire Management. *J. For. Res.* **2005**, *16*, 73–78. [CrossRef]
16. Wooster, M.J.; Roberts, G.J.; Giglio, L.; Roy, D.P.; Freeborn, P.H.; Boschetti, L.; Justice, C.; Ichoku, C.; Schroeder, W.; Davies, D.; et al. Satellite Remote Sensing of Active Fires: History and Current Status, Applications and Future Requirements. *Remote Sens. Environ.* **2021**, *267*, 112694. [CrossRef]

17. Saltikoff, E.; Friedrich, K.; Soderholm, J.; Lengfeld, K.; Nelson, B.; Becker, A.; Hollmann, R.; Urban, B.; Heistermann, M.; Tassone, C. An Overview of Using Weather Radar for Climatological Studies: Successes, Challenges, and Potential. *Bull. Am. Meteorol. Soc.* **2019**, *100*, 1739–1752. [CrossRef]
18. Doviak, R.J.; Zrnić, D.S. *Doppler Radar and Weather Observations*, 2nd ed.; Academic Press: San Diego, CA, USA, 1993; 562p, ISBN 978-0122214226.
19. Melnikov, V.M.; Zrnić, D.S.; Rabin, R.M.; Zhang, P. Radar polarimetric signatures of fire plumes in Oklahoma. *Geophys. Res. Lett.* **2008**, *35*, L14811. [CrossRef]
20. McCarthy, N.; Guyot, A.; Dowdy, A.; McGowan, H. Wildfire and Weather Radar: A Review. *J. Geophys. Res. Atmos.* **2019**, *124*, 266–286. [CrossRef]
21. Lang, T.J.; Rutledge, S.A.; Dolan, B.; Krehbiel, P.; Rison, W.; Lindsey, D.T. Lightning in Wildfire Smoke Plumes Observed in Colorado during Summer 2012. *Mon. Weather Rev.* **2014**, *142*, 489–507. [CrossRef]
22. Lareau, N.P.; Donohoe, A.; Roberts, M.; Ebrahimian, H. Tracking Wildfires with Weather Radars. *J. Geophys. Res. Atmos.* **2022**, *127*, e2021JD036158. [CrossRef]
23. Shu, S.; Chen, Y.; Cao, S.; Zhang, B.; Fang, C.; Xu, J. Monitoring and Alarm Method for Wildfires near Transmission Lines with multi-Doppler Weather Radars. *IET Gener. Transm. Distrib.* **2023**, *17*, 2055–2069. [CrossRef]
24. Zrnic, D.; Zhang, P.; Melnikov, V.; Mirkovic, D. Of Fire and Smoke Plumes, Polarimetric Radar Characteristics. *Atmosphere* **2020**, *11*, 363. [CrossRef]
25. Krishna, M.; Saide, P.E.; Ye, X.; Turney, F.A.; Hair, J.W.; Fenn, M.; Shingler, T. Evaluation of Wildfire Plume Injection Heights Estimated from Operational Weather Radar Observations Using Airborne Lidar Retrievals. *J. Geophys. Res. Atmos.* **2024**, *129*, e2023JD039926. [CrossRef]
26. Bian, R.; Chen, K.; Li, G.; Wang, Z.; Qiu, Y.; Bai, H.; Kong, W. Evaluation of Three Algorithms and Forest Fire Risk Prediction in Zhejiang Province of China. *Forests* **2024**, *15*, 2146. [CrossRef]
27. Li, X.; Liu, L.; Qi, S. Forest Fire Hazard during 2000–2016 in Zhejiang Province of the Typical Subtropical Region, China. *Nat. Hazards* **2018**, *94*, 975–977. [CrossRef]
28. Chen, Z.; Wang, M.; Zhang, H.; Lin, S.; Guo, Z.; Jiang, Y.; Zhou, C. Long-Term Change in Low-Cloud Cover in Southeast China during Cold Seasons. *Atmos. Ocean. Sci. Lett.* **2022**, *15*, 100222. [CrossRef]
29. Yang, Y.; Zhao, C.; Fan, H. Spatiotemporal Distributions of Cloud Properties over China Based on Himawari-8 Advanced Himawari Imager Data. *Atmos. Res.* **2020**, *240*, 104927. [CrossRef]
30. Jang, E.; Kang, Y.; Im, J.; Lee, D.-W.; Yoon, J.; Kim, S.-K. Detection and Monitoring of Forest Fires Using Himawari-8 Geostationary Satellite Data in South Korea. *Remote Sens.* **2019**, *11*, 271. [CrossRef]
31. Phiri, D.; Simwanda, M.; Salekin, S.; Nyirenda, V.R.; Murayama, Y.; Ranagalage, M. Sentinel-2 Data for Land Cover/Use Mapping: A Review. *Remote Sens.* **2020**, *12*, 2291. [CrossRef]
32. Yang, Z.; Qi, Y.; Zhang, Z.; Li, D. Can CINRAD Radar With VCP-21 Mode Capture the Accumulated Rainfall Pattern and Intensity of Fast-Moving Storms? *IEEE Trans. Geosci. Remote Sens.* **2024**, *62*, 4100813. [CrossRef]
33. Oh, Y.-A.; Kim, H.-L.; Suk, M.-K. Clutter Elimination Algorithm for Non-Precipitation Echo of Radar Data Considering Meteorological and Observational Properties in Polarimetric Measurements. *Remote Sens.* **2020**, *12*, 3790. [CrossRef]
34. Fabry, F. *Radar Meteorology: Principles and Practice*; Cambridge University Press: Cambridge, UK, 2015; 552p, ISBN 978-1107024961.
35. National Weather Service. Field Guide Glossary: D's. Available online: https://www.weather.gov/spotterguide/glossary_d (accessed on 23 July 2025).
36. Duff, T.J.; Chong, D.M.; Penman, T.D. Quantifying Wildfire Growth Rates Using Smoke Plume Observations Derived from Weather Radar. *Int. J. Wildland Fire* **2018**, *27*, 514–524. [CrossRef]
37. Park, H.S.; Ryzhkov, A.V.; Zrnić, D.S.; Kim, K.-E. The Hydrometeor Classification Algorithm for the Polarimetric WSR-88D: Description and Application to an MCS. *Weather Forecast.* **2009**, *24*, 730–748. [CrossRef]
38. Martin, W.J.; Shapiro, A. Discrimination of Bird and Insect Radar Echoes in Clear Air Using High-Resolution Radars. *J. Atmos. Ocean. Technol.* **2007**, *24*, 1215–1230. [CrossRef]
39. Deng, M.; Volkamer, R.M.; Wang, Z.; Snider, J.R.; Kille, N.; Romero-Alvarez, L.J. Wildfire Smoke Observations in the Western United States from the Airborne Wyoming Cloud Lidar during the BB-FLUX Project. Part II: Vertical Structure and Plume Injection Height. *J. Atmos. Ocean. Technol.* **2022**, *39*, 545–558. [CrossRef]
40. Pandžic, M.; Mihajlovic, D.; Pandžic, J.; Pfeifer, N. Assessment of the geometric quality of sentinel-2 data. *Int. Arch. Photogramm. Remote Sens. Spat. Inf. Sci.* **2016**, *XLI-B1*, 489–494. [CrossRef]
41. Liu, X.; He, B.; Quan, X.; Yebra, M.; Qiu, S.; Yin, C.; Liao, Z.; Zhang, H. Near Real-Time Extracting Wildfire Spread Rate from Himawari-8 Satellite Data. *Remote Sens.* **2018**, *10*, 1654. [CrossRef]
42. Aydell, T.B.; Clements, C.B. Mobile Ka-band polarimetric Doppler radar observations of wildfire smoke plumes. *Mon. Weather Rev.* **2021**, *149*, 2827–2844. [CrossRef]

43. Melnikov, V.M.; Zrnic, D.S.; Rabin, R.M. Polarimetric Radar Properties of Smoke Plumes: A Model. *J. Geophys. Res. Atmos.* **2009**, *114*, D21. [CrossRef]
44. Koo, E.; Linn, R.R.; Pagni, P.J.; Edminster, C.B. Modelling Firebrand Transport in Wildfires Using HIGRAD/FIRETEC. *Int. J. Wildland Fire* **2012**, *21*, 396–417. [CrossRef]
45. Melnikov, V.; Zrnic, D.; Free, A.; Ice, R.; Macemon, R. *Monitoring Radar Calibration Using Ground Clutter*; NOAA/National Severe Storms Laboratory: Norman, OK, USA, 2017.

Disclaimer/Publisher's Note: The statements, opinions and data contained in all publications are solely those of the individual author(s) and contributor(s) and not of MDPI and/or the editor(s). MDPI and/or the editor(s) disclaim responsibility for any injury to people or property resulting from any ideas, methods, instructions or products referred to in the content.